Competitive screening and band gap renormalization in *n*-type monolayer transition metal dichalcogenides

S. Samaneh Ataei* and Ali Sadeghi†
Department of Physics, Shahid Beheshti University, Tehran, Iran

(Received 7 June 2021; revised 15 September 2021; accepted 20 September 2021; published 4 October 2021)

Gate induced carriers impact the many-body interactions in monolayer transition metal dichalcogenides (TMDs) by modifying the screened Coulomb potential and renormalizing the band gap, thus influencing the strong excitonic effects in these materials. Using the *GW* approximation and a plasmon pole theory to model the carrier induced plasmons in the frequency-dependent part of the screening, we accurately calculate the band gap renormalization of the electron doped monolayer MoS_2 and WS_2. The excitonic states of the low doped systems are calculated by solving the Bethe-Salpeter equation. Our results clarify the competition between screening and band gap renormalization. An exact cancellation occurs between the reduced band gap and the exciton binding energy for doped monolayer WS_2, in good agreement with previous experimental results. In contrast, the exciton energy of doped monolayer MoS_2 blueshifts by tens of meV. We show the role of the electronic band structure of the monolayers in the calculated exciton energies. Our results could be generally expanded to other monolayer TMDs and are helpful for quantitatively engineering optoelectronic devices with desired features.

DOI: 10.1103/PhysRevB.104.155301

I. INTRODUCTION

Transition metal dichalcogenides (TMDs) are layered structures with unique electronic and optical properties [1–3]. Reduced screening results in the formation of tightly bound excitons in these materials with remarkable excitonic effects [3–5]. Monolayer TMD semiconductors, showing a controllable large exciton binding energy and giant renormalization of band gap [6,7], promise applications in room-temperature optoelectronics. To become applicable in optoelectronic devices, their optical properties can be tuned by different strategies which would in turn affect many-body interactions. Doping with free carriers, e.g., gate control of carriers [8–10], is a strategy that probes the higher order excitations such as trions [11,12] on one hand, and influences the spectral position of the neutral exciton on the other hand. The optical spectra and excitonic effects are affected by carrier doping through several mechanisms such as Pauli blocking and screening of the Coulomb interaction. The former raises the electron-hole continuum energy and leads to the reduction of the exciton binding energy due to the occupation of electronic states and the electron's fermionic nature. The latter, on the other hand, is the most important effect at low doping concentrations [13]. Doping weakens the Coulomb interaction and hence lowers the exciton binding energy and causes the renormalization of the band gap. The competition between these two factors, which is the focus of the present paper, will determine the exciton energy. For instance, it has been observed experimentally that the exciton energy blueshifts with doping though the blueshift is negligible at low doping concentrations [11,14]. A nonlinear behavior of the renormalized band gap has also been observed for doped monolayer TMDs [15].

For describing these observed phenomena and revealing the doping effects on microscopic behavior of physical quantities in two-dimensional (2D) semiconductors, one has to consider many-body interactions in the *ab initio* calculations. The *GW*+Bethe-Salpeter equation (BSE) has been proven as a powerful method to accurately describe the quasiparticle (QP) and optical absorption spectra of the undoped 2D layered structures [4,16]. However, applying this approach to the doped 2D systems is more challenging as it suffers from the requirement of a very dense k-point sampling for capturing the subtle electron occupancies. Indeed, the frequency dependent part of the dielectric function has to be taken into account with caution because of the appearance of low energy plasmons in the doped systems that may raise the need to a full frequency calculation of the dielectric function which is too demanding. However, taking into account the low energy plasmon interactions and the *GW* approximation, an efficient plasmon pole theory was identified by Liang and Yang [17]. Based on that an effective mass approximation was developed to model the dielectric function in terms of intrinsic polarizability and the polarizability of a 2D electron gas that is calculated analytically and reduces the requirements of k-point sampling in calculating the band gap renormalization of doped systems [18]. It has been shown that the change to the screened Coulomb potential, concentrating on the head part of the static screening at small $\mathbf{q}$, plays an important role in determining the change to the self-energy and hence the renormalized band gap of a doped system [17,18]. It was also found that the dynamical screening effects are important in calculating the excitonic features of doped systems [19].

In the present paper, we consider the *GW* self-energy, with the widely used general plasmon-pole model [20] for the dynamically screened potential, to calculate the QP energies

*sataei@nano.cnr.it; s_ataei@sbu.ac.ir
†ali_sadeghi@sbu.ac.ir

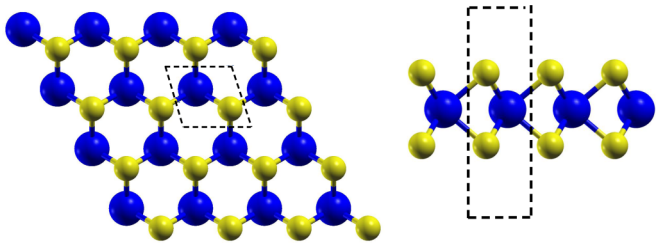

FIG. 1. Top and side views of monolayer XS_2 where X (= Mo or W) atoms are shown by blue larger spheres while the S atoms are shown by yellow smaller ones. One unit cell is indicated by the dashed box.

of the undoped systems. In order to accurately calculate the renormalized band gap of the doped systems, we apply the low doped asymptotic limit of the *GW* self-energy modeled with the plasmon pole theory [17]. Our calculations take advantage of using *ab initio* calculation data points as input in the self-energy in an efficient way by applying the asymptotic behavior of the *GW* self-energy and a correct description of the head part of the screening at small $\mathbf{q}$. Our calculated nonlinear behavior of band gap renormalization of doped monolayer MoS_2 is in very good agreement with fully *ab initio* calculations [17] and also the recently reported experimental results at low concentrations [15]. The head part of the screening at small $\mathbf{q}$ not only plays an important role in determining the change to the self-energy (mentioned above) but also is very important in BSE calculations of the doped systems. The static screened Coulomb potential included in the BSE kernel contains both intra- and interband transitions and the head part of it is correctly described at the metallic limit ($\mathbf{q} \to 0$) (see Appendix B). Interestingly, we found different behavior for the exciton energy of doped monolayers MoS_2 and WS_2 at low concentrations. Our calculations show an exact cancellation between the reduced band gap and exciton binding energy for monolayer WS_2 and a blueshift within tens of meV for the first strongest exciton energy of monolayer MoS_2. The latter might occur due to not considering dynamical screening effects, i.e., because of Pauli blocking effects, as previously reported [19]. However, a different electronic band structure of monolayer WS_2 results in an almost unchanged exciton energy associated with empty subbands, well reproducing the measured optical absorption spectra, thus indicating a negligible impact of dynamical corrections to the screening. Our calculated results could be generally applied to all monolayer TMDs with single particle electronic structures similar to MoS_2 and WS_2. Our findings might also help to clarify how to apply GW+BSE calculations in 2D semiconductors with metallic contributions to the screening.

II. COMPUTATIONAL DETAILS

Two prototypelike TMD model systems, namely, monolayers of MoS_2 and WS_2 as depicted in Fig. 1, are investigated in this paper. The lattice constant of WS_2 is set to 3.16 Å [21,22] while for MoS_2 it is set to 3.19 Å, i.e., the same as that of bulk MoS_2 at zero pressure [23]. The supercell method is used to model the 2D structures with a vacuum gap in the normal-to-plane direction of height about 16 Å, large enough to prevent interactions between periodic images along this direction.

First-principles ground-state calculations are performed based on the density functional theory (DFT) within the Perdew-Burke-Ernzerhof (PBE) approximation of the exchange-correlation (XC) functional [24] as implemented in the QUANTUM ESPRESSO code package [25]. Our results are considered well converged with a cutoff of 100 Ry for expanding the wave function in terms of plane waves. We consider optimized norm conserving Vanderbilt pseudopotentials [26] to replace all the core states of S ($3s^2, 3p^4$) and some deep ones of Mo ($4s^2, 4p^6, 4d^4, 5s^2$) and W ($4f^{14}, 5s^2, 5p^6, 5d^4, 6s^2$). Spin-orbit coupling is included in the calculations as it plays a significant role in the electronic structure of TMDs and leads, for instance, to the splitting of the two top valence bands [27,28]. Electron doping in doped systems is modeled as an increased total number of electrons (up to 0.01 electron per unit cell) while a compensating jellium background of an opposite charge is also added to the simulation box for technical reasons in DFT calculations.

We further perform *GW* calculations to obtain accurate QP energies [29,30] as implemented in YAMBO code [31]. We employ the widely used non-self-consistent variant, i.e., the G_0W_0 approximation, where the self-energy of the many-body electronic system $\Sigma \approx iG_0W_0$ is calculated on top of the single-particle Kohn-Sham eigenvalues. The dynamically screened Coulomb interaction W is approximated with the plasmon pole model [20] which has been proven to work well in the case of semiconductors. The box-shaped cutoff [32] has been applied to treat the long range limit of the Coulomb potential which may cause spurious interactions between periodic images. We verified that the calculated QP energies of the pristine monolayers are well converged (see Appendix A) with respect to the sampling resolution of the k grid (36×36), total number of bands (200) used for the summation to build the polarizability, and the kinetic energy cutoffs of the exchange and correlation parts of the self-energy (60 and 10 Ry, respectively).

Finally, the optical absorption spectra and excitation energies are calculated by solving the BSE considering the particle-hole interaction implemented in YAMBO code [31]. The static screening in the direct term is calculated within the random phase approximation (RPA) by inclusion of local field effects with energy cutoff of 10 Ry (see Appendix A). We adopt the metallic limit for doped semiconductors as will be explained in Appendix B. Converged excitation energies are obtained with three valence and three conduction bands in the Bethe-Salpeter matrix, the irreducible Brillouin zone being sampled with a 48×48 k-point grid. The convergence of excitation energy and exciton binding energy with respect the k-point grid has been addressed in Appendix A.

III. RESULTS AND DISCUSSION

In the following, we study the absorption spectra, excitonic effects, and modulation of the band gap energy of electron doped systems, all of which will then be investigated and discussed. Note that the electronic band structures of pristine monolayer MoS_2 and WS_2, presented in Fig. 2, indicate a direct gap at the K point of the Brillouin zone. We therefore restrict our study to this point in this paper.

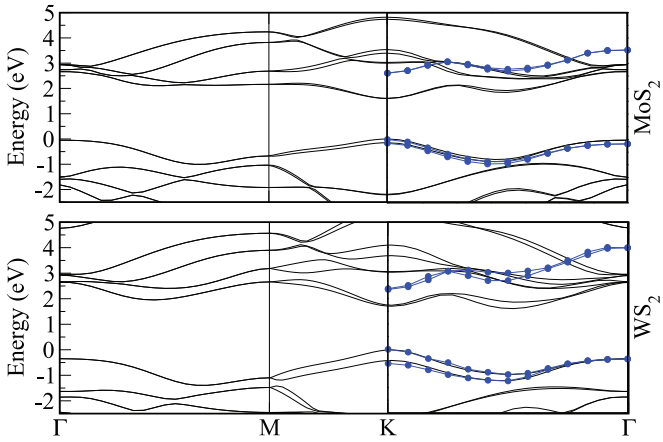

FIG. 2. Electronic band structures of undoped monolayer MoS_2 (top) and WS_2 (bottom) from PBE calculations (thin continuous lines). For comparison, QP energies from *GW* calculations are also shown for a few representative k points along the $K - \Gamma$ path for two topmost valence bands and two bottommost conduction bands. The valence band maximum is offset to zero in all cases for convenience.

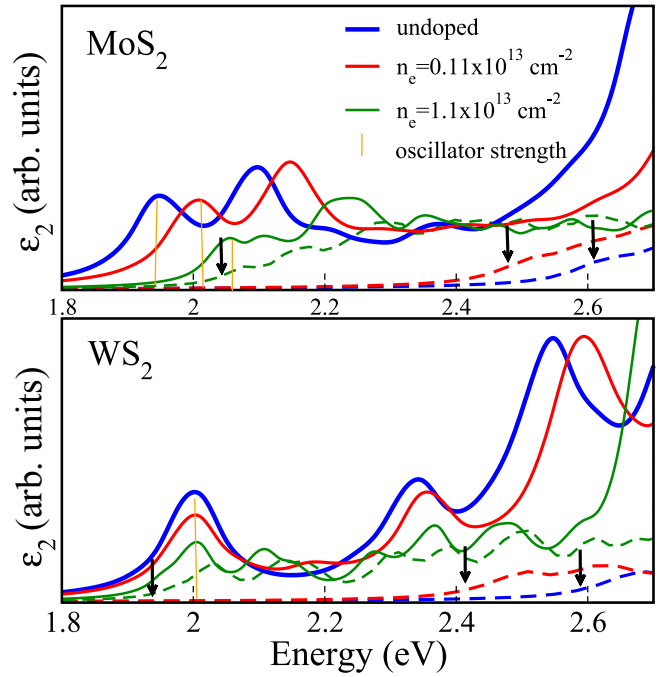

FIG. 3. Optical absorption spectra (the imaginary part of the dielectric function vs photon energy) of pristine (thick blue curve) and doped (thin red and green curves) monolayer MoS_2 and WS_2 with an applied Lorentzian broadening of 0.05 eV. The relative oscillator strength of the first strongest exciton from the BSE calculations (continuous lines) is shown by the vertical orange lines while the QP band gaps from RPA calculations (dashed lines) are indicated by arrows. The spectra of WS_2 are shifted by about 0.2 eV to become comparable with the experimental data in Ref. [33].

A. Absorption spectra and excitonic effects

As screening plays the dominant role in both excitonic effects and band gap renormalization, we calculate the absorption spectra and exciton binding energy by solving the BSE and the renormalized QP band gap using *GW* self-energy (see Sec. III B), respectively. We inspect how the screening affects the absorption of low doped monolayer MoS_2 and WS_2. The static screened Coulomb potential included in the BSE kernel contains the interband and intraband transitions for every finite $\mathbf{q}$ whereas only the interband transitions are included in YAMBO code [31] for the $\mathbf{q} = 0$ component. As explained in Appendix B, the screening can be correctly described also at this metallic limit, which is critically important in the present case that extra electrons dope the 2D semiconductor. Applying this correction, we calculate the absorption spectra of the doped monolayer MoS_2 and WS_2 as shown in Fig. 3. The absorption spectra of the undoped structure of the considered monolayers are also shown as a reference. Note that a scissor operator obtained from the *GW*-calculated renormalized band gap (see Sec. III B) is applied as a correction to the PBE eigenvalues. Although the valence and conduction band dispersion changes are not considered we have checked for the excitonic spectrum of undoped monolayer MoS_2 that the difference to a BSE calculation based on *GW* energies is negligible.

Notably, it is seen in Fig. 3 that electron doping induces a redshift to the RPA spectrum onset which is a result of the band gap reduction. Solving the BSE with electron-hole interaction, on the other hand, the first strongest exciton resonances of monolayer MoS_2 blueshift by about 50 and 100 meV due to the two low electron doping concentrations $n_e = (0.11, 1.1) \times 10^{13}$ cm^{-2}, corresponding to 0.001 and 0.01 electrons per unit cell, respectively. Interestingly, no such blueshift is observed for monolayer WS_2 for either of the concentrations. The predicted cancellation in doped monolayer WS_2 is fairly consistent with the previous experimental observations [34].

The calculated redshift of the RPA spectra onset and/or the exciton energy blueshifts clearly shows that the exciton binding energy reduces with increasing the doping. This is verified also by visualizing the square modulus of the exciton wave function (first peak at the low energy region) shown in Fig. 4, where the electron bound to the hole becomes more delocalized upon electron doping. Interestingly, both investigated monolayer TMDs share this feature, indicating a reduced exciton binding energy due to electron doping of TMDs. Based on our calculations, the exciton binding energy decreases by about 190 and 180 meV in monolayer MoS_2 and WS_2, respectively, doped by $n_e = 0.11 \times 10^{13}$ cm^{-2}. The exciton is completely ionized at $n_e = 1.1 \times 10^{13}$ cm^{-2} in monolayer WS_2.

We attribute the emergent dissimilarity, i.e., the exciton energy blueshift in doped MoS_2 as opposed to exact cancellation in doped WS_2, to the different electronic structures of the two addressed monolayers. As schematically depicted in Fig. 5, the bright exciton transition shown by arrows depends on the band structure at the K point. However, the band structures of the two test case monolayers deform in different ways in response to doping. Shown as insets in the left panels in Fig. 5 is the conduction band minimum (CBM) state of the pristine monolayers calculated with the PBE functional which features in both cases the d_{z^2} orbital localized on the metal atom. We put as the corresponding insets of the right panels in Fig. 5 the electron density difference between the doped and pristine

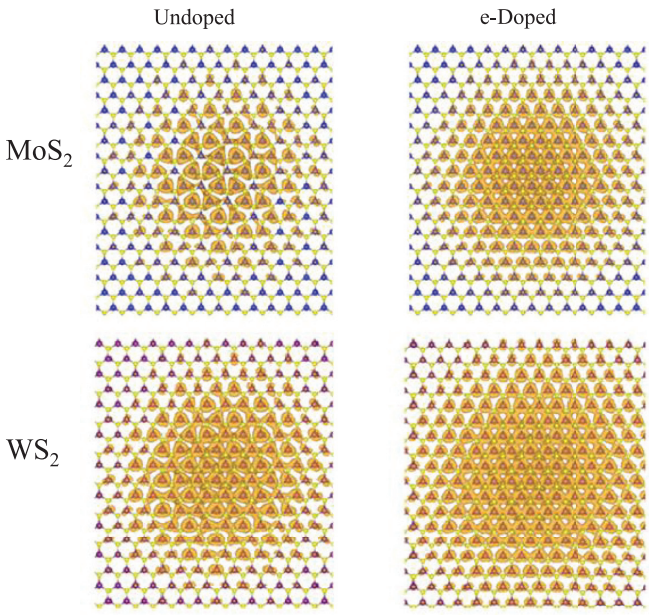

FIG. 4. Square modulus of the wave function of the first strongest exciton for pristine (left) and doped (right) monolayer MoS_2 (top) and WS_2 (bottom) with $n_e = 1.1 \times 10^{12}$ cm^{-2}. The hole is frozen at the center so the delocalized spot visualizes the probability of finding the bound electron to it. Only the central region of the 27×27 supercell is shown.

monolayers. It is evident that the electrons injected into the monolayers reside localized on the Mo and W atoms although the spatial distribution of the excess electrons mimics only imperfectly the d_{z^2} nature of the CBM states of the undoped samples. The energy of the partially filled CBM states (with an occupancy of $\simeq 0.01$ from our DFT calculations for a

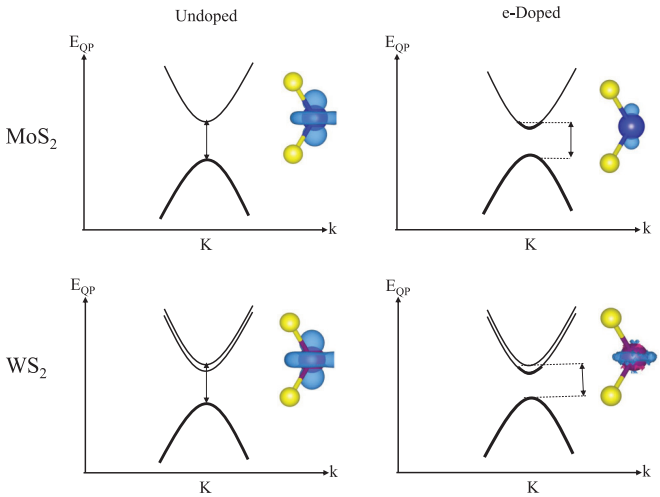

FIG. 5. Schematic representation of the evolution of the electronic band structures and exciton transitions of monolayer MoS_2 and WS_2 from pristine (left) to low electron doped (right). The arrows indicate the electron-hole transition associated with the first strongest exciton. The insets show the CBM at the K point from PBE calculations for undoped samples (left) or the doping-induced electron density difference as an isosurface of 10^{-4} e/bohr^3 (right) to visualize the spatial distribution of the excess electron.

concentration of 0.01 e per unit cell) is expected to downshift after the doping and the gap is thus narrowed (see Sec. III B).

However, a spin splitting occurs at the K point for the monolayer WS_2. According to our PBE (QP) calculations, the split states of pristine WS_2 differ by about 40 (10) meV. Similar to MoS_2, the lower-lying conduction band state is partially filled by the doping electrons and experiences an energy downshift. Based on our DFT calculations, doping the monolayer WS_2 with an electron concentration of 0.01 e per unit cell, almost all ($\simeq 99\%$) of the excess electrons reside in the lower conduction band. The exciton transition is associated with the higher-lying conduction band which remains unoccupied (to within 10^{-4} e). The latter is consistent with experimental results reported by Chernikov *et al.* [34], who ruled out Pauli blocking in monolayer WS_2. In contrast, Pauli blocking and hence a raise in electron-hole continuum energy occurs in monolayer MoS_2 [19], leading to a blueshift of the excitation energy. Gao *et al.* [19] suggested that the calculated blueshift in monolayer MoS_2 could be cured by treating the dynamical corrections to the static dielectric function to reproduce the cancellation. An important outcome from our results above is that the dynamical corrections to the static dielectric function play no role in the low doped monolayer WS_2 without Pauli blocking effects. Our results might also shed light on the observed difference between the increased amount of blueshifts in monolayer $MoSe_2$ and WSe_2 with increasing electron doping [14].

B. Band gap renormalization

As already argued in Sec. III A, the observed exact cancellation effect occurs as a result of simultaneous reduction of band gap and the exciton binding energy in doped monolayer WS_2. This highlights the importance of investigation of the band gap renormalization of doped TMDs. It has been observed that the band gap of 2D TMDs gets narrower as the electron doping increases and finally saturates for large carrier concentrations [15]. To shed some light on the origin of the observed nonlinear behavior of band gap renormalization of monolayer TMDs, we next conduct a series of calculations with electron doping concentrations up to 1.1×10^{13} cm^{-2} that are commonly used in experiments [35]. In the DFT calculations, electron doping is modeled as an increased total number of electrons (up to 0.01 electron per unit cell) while a compensating jellium background of an opposite charge is also added to the simulation box for technical reasons. Note that the ground-state DFT calculations with the PBE type of XC functional show only a marginal dependence of the band gap on the doping concentration. For example, for a moderate concentration of 1.1×10^{13} cm^{-2} introduced to monolayer MoS_2, the calculated Hartree contribution to the change of the band gap is 10 meV while the XC contribution is -6 meV. In fact, the excess electrons added to the conduction band increase the Hartree repulsion while they lead to decrement of the XC energy.

In order to correctly describe the many-electron properties beyond the standard DFT calculations, e.g., the charged excitations needed to compute the energy band gap, we consider the *GW* self-energy to calculate QP energies of the doped systems. The correcting terms due to the excess electrons are

added to the G_0W_0 self-energy of the intrinsic 2D structures. Once the system is doped by electrons, the intrinsic self-energy changes due to the increased screening effects, which is effectively described by δW. The latter induces in turn a change in the intrinsic Green's function as δG. The self-energy can therefore be split up into the intrinsic $\Sigma_{\rm int} = iG_{\rm int}W_{\rm int}$ and some doping-induced extrinsic contributions [17]:

$$\begin{aligned}\Sigma &= \Sigma_{\rm int} + \Sigma_{\rm ext} \\ &= i(G_{\rm int}W_{\rm int} + G_{\rm int}\delta W + \delta G W_{\rm int} + \delta G \delta W). \end{aligned} \tag{1}$$

Our calculations show that the sum of the last two terms in Eq. (1) is -13 meV for a concentration of 1.1×10^{13} cm^{-2}, i.e., negligible, in agreement with previous calculations [17]. We will therefore keep only one dominant term in the extrinsic self-energy $\Sigma_{\rm ext} \simeq iG_{\rm int}\delta W$. Plasmon resonance due to the excess electrons modifies the frequency-dependent part of the screening. Here, we follow the plasmon pole model introduced by Gao amd Yang [18], $\delta\varepsilon_{00}^{-1}(\mathbf{q},\omega) = \frac{\delta\varepsilon_{00}^{-1}(\mathbf{q},0)\omega_d^2(\mathbf{q})}{\omega^2-\omega_d^2(\mathbf{q})}$, where $\delta\varepsilon_{00}^{-1}(\mathbf{q},0)$ is the difference between the head part of the static dielectric functions of the doped and intrinsic monolayer while $\omega_d(\mathbf{q})$ is the plasmon frequency. The resulting self-energy reads

$$\Sigma_{\rm ext}^{n\mathbf{k}}(E) = \pm\int \frac{d\mathbf{q}}{(2\pi)^2}|M_{nn}(\mathbf{k}-\mathbf{q},0)|^2 \times \frac{\delta\varepsilon_{00}^{-1}(\mathbf{q},0)}{2\left(1\pm\frac{\varepsilon_{n,\mathbf{k}-\mathbf{q}}-E}{\omega_d(\mathbf{q})}\right)}v_{\rm 2D}(\mathbf{q}) \tag{2}$$

where $+$ and $-$ correspond to the conduction and valence states, respectively, while M_{nn} denotes the plane wave matrix elements. In the low density limit and within the on-shell approximation to the self-energy, a rigid shifting of the whole resonance profile along the energy axis, the asymptotic behavior of the self-energy attributed to the valence band maximum (VBM) and CBM is calculated as [18]

$$\begin{aligned}\Sigma_{\rm ext}^{\rm CBM/VBM} &\simeq \pm\int \frac{d\mathbf{q}}{(2\pi)^2}\frac{\delta\varepsilon_{00}^{-1}(\mathbf{q},0)}{2[1\pm\frac{\varepsilon_{\mathbf{q}}}{\omega_d(\mathbf{q})}]}v_{\rm 2D}(\mathbf{q}) \\ &= \pm\int \frac{d\mathbf{q}}{(2\pi)^2}\frac{\delta W_{00}(\mathbf{q},0)}{2[1\pm\frac{\varepsilon_{\mathbf{q}}}{\omega_d(\mathbf{q})}]} \end{aligned} \tag{3}$$

where $\delta W_{00}(\mathbf{q},0) = \delta\varepsilon_{00}^{-1}(\mathbf{q},0)v_{\rm 2D}(\mathbf{q}) = W_{00}(\mathbf{q},0) - W_{00,\rm int}(\mathbf{q},0)$ while $\omega_d(\mathbf{q}) \approx \sqrt{2\pi nq/m}$ is the plasmon dispersion relation of a 2D electron gas with an effective mass m and doping concentration n, and finally ε_q is the energy eigenvalue obtained from the PBE calculations. We use *ab initio* calculations to find the integrand, i.e., static dielectric function and hence screened interaction, on a set of $\mathbf{q}$ points as inputs for the integrals. The static dielectric function is calculated on a 48×48 k mesh. The calculated electron and hole effective masses are listed in Table I.

We calculate the energy gap of the doped system as

$$E_{\rm g} = E_{\rm g,int} + \Sigma_{\rm ext}^{\rm CBM} - \Sigma_{\rm ext}^{\rm VBM} \tag{4}$$

and ignore the small changes predicted in PBE calculations of the doped system. The renormalized energy gap and corresponding extrinsic self-energies with separated VBM and CBM contributions, calculated for doped MoS_2 and WS_2 monolayers, are shown in Fig. 6 as a function of doping concentration. A considerable monotonic reduction of the band gap is observed by increasing the electron doping. Our calculated renormalized band gap of 2.2 eV, as a result of a band gap reduction of ≈0.4 ev, for the doping concentration of 5.5×10^{12} cm^{-2} in monolayer MoS_2 well reproduces the previous calculated [18] and also experimentally measured data [15]. However, increasing the doping density to 1.1×10^{13} cm^{-2} the calculated band gap reduction reaches ≈0.57 eV for the monolayer MoS_2, showing a good consistency with the measured data [15]. A similar behavior is observed for monolayer WS_2 with a band gap reduction of about 0.65 eV. Using the widely used general plasmon pole model [20], we have also calculated the renormalized band gap of the doped monolayer MoS_2 at doping concentration of 0.11×10^{13} cm^{-2} and found a band gap of 2.457 eV which is slightly smaller (20 meV) than the one we calculated with the model described above. Here, we have been able to explain the nonlinear behavior of the band gap renormalization with respect to electron doping in terms of the extrinsic self-energy which causes a reduction of CBM energy and in turn enhancement of VBM energy at low concentrations. These results again show that the change of screening due to adding electrons plays an important role in band gap renormalization of monolayer MoS_2 and WS_2.

Furthermore, because of the similar effective masses of electron and hole we expect a similar behavior of band gap renormalization in hole doped systems where we calculated a band gap reduction of about 154 meV for the hole doped monolayer WS_2 with a concentration of 1.1×10^{12} cm^{-2}.

TABLE I. Calculated electron and hole effective masses in MoS_2 and WS_2 monolayers with respect to the free electron mass m_0.

System	Point	m_h/m_0	m_e/m_0
MoS_2	K	−0.53	0.48
WS_2	K	−0.39	0.42

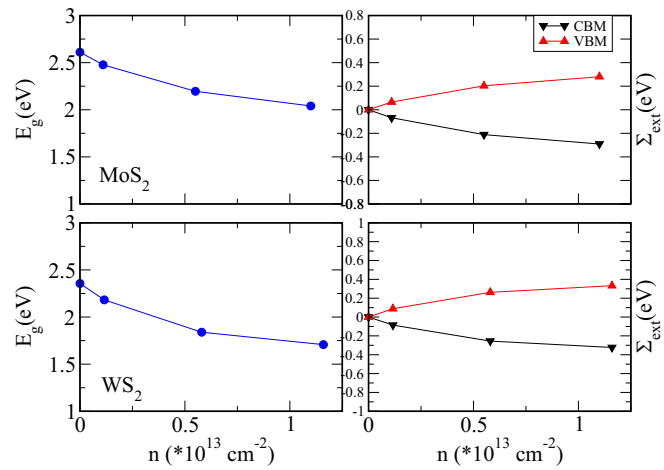

FIG. 6. The calculated band gap renormalization and corresponding extrinsic self-energy (related to VBM and CBM) of doped monolayer MoS_2 and WS_2 as a function of doping concentration.

IV. CONCLUSION

Gate control of carrier concentration causes considerable tunability of physical properties in 2D structures. In particular, the presence of free charge carriers in the system can influence the exciton binding energy and the QP band gap. It has been interestingly observed that at low doping concentrations the exciton resonance energies of monolayer TMDs remain almost unchanged and blueshift linearly with increasing the doping. The unchanged exciton resonance energies of a low doped monolayer show a cancellation effect between the renormalized band gap and the exciton binding energy.

Here, we have calculated the band gap renormalization and excitonic properties of free electron doped monolayers MoS_2 and WS_2, for which the competition between band gap reduction and screening at low concentrations results in a blueshift or almost no change of the exciton energy. Using *GW* approximation for the self-energy and considering the static dielectric function to construct an electron hole kernel in BSE calculations, we show an exact cancellation occurs between the reduced band gap and exciton binding energy in monolayer WS_2, while the exciton energy of monolayer MoS_2 blueshifts within tens of meV. This difference might emerge due to the single particle electronic structure of W based and Mo based systems. These findings might shed light on the observed different amount of the blueshifts for monolayer WSe_2 and $MoSe_2$ with increasing the doping. Our results would also be helpful for engineering optoelectronic devices with gate control of carriers. The treated *GW*+BSE methodology we used in this paper could be useful for modeling 2D semiconductors with metallic contributions to the screening.

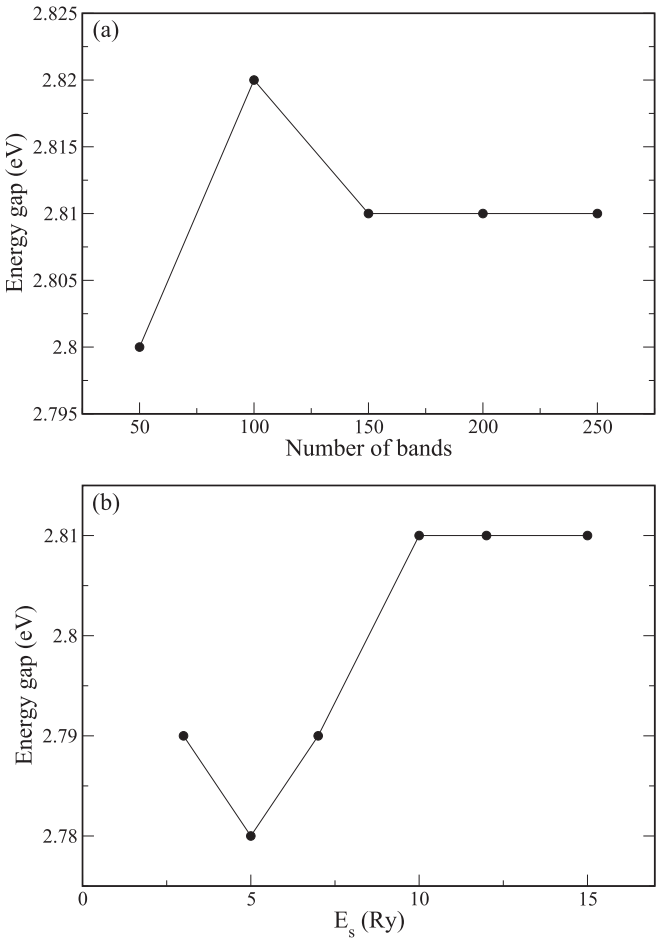

FIG. 7. (a) *GW* convergence of the quasiparticle band gap (at the K point) of undoped monolayer MoS_2 as a function of the number of bands used for the sum over states. We used a $18\times18\times1$ k-point grid sampling and a 10-Ry energy cutoff for the dielectric matrix. In all calculations the technique to accelerate the convergence with respect to empty bands proposed by Bruneval and Gonze [36] was adopted. (b) The same convergence test with respect to the energy cutoff (matrix dimension) of the dielectric matrix (E_s) using a $18\times18\times1$ k mesh and summing over 200 bands with the accelerated technique of Ref. [36].

ACKNOWLEDGMENTS

S. Samaneh Ataei thanks Dr. Daniele Varsano for his valuable comments and suggestions, and acknowledges access to the Marconi supercomputing system based at CINECA, Italy through the Italian ISCRA program. Computational resources were partially provided by the SARMAD cluster at SBU.

APPENDIX A: CONVERGENCE TESTS

When investigating the quasiparticle band structure and optical properties of monolayers with a two-dimensional structure, it is important to use a well converged energy cutoff (i.e., the matrix dimension of the dielectric matrix) and k-grid sampling. In particular, the strong dependence of the dielectric function on momentum $\mathbf{q}$ in the long wavelength region implies that a denser k-points grid is needed to converge the quasiparticle band gaps and exciton binding energies. Here we show in detail the convergence tests done for both quasiparticle and exciton energies reported in the main text.

It can be seen from Fig. 7(a) that the usage of the accelerate technique, proposed by Bruneval and Gonze [36], allows us to achieve quasiparticle gaps converged already using 200 bands.

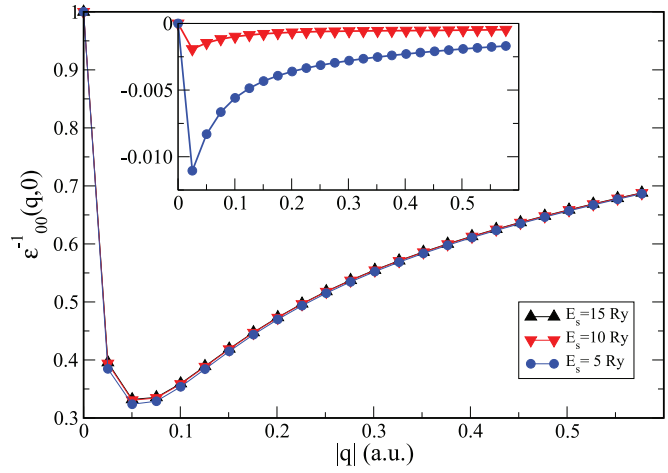

FIG. 8. Static inverse dielectric function of undoped monolayer MoS_2 calculated in the RPA, for several finite $|\mathbf{q}|$ along the $\Gamma-M$ direction, with various energy cutoffs of the dielectric matrix (E_s). The static inverse dielectric function of undoped monolayer MoS_2 with E_s=15 Ry has been set to zero in the inset.

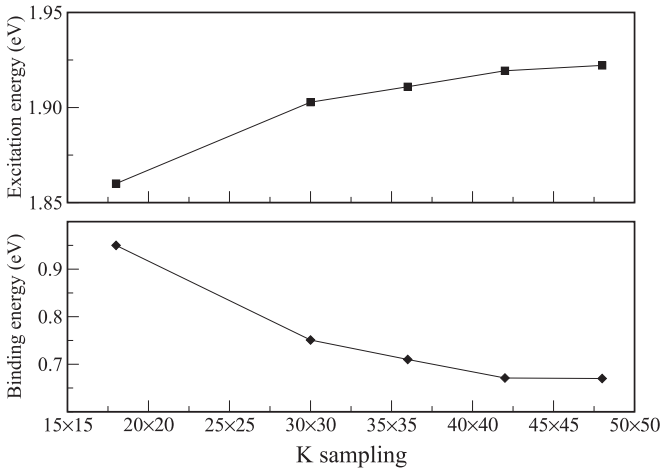

FIG. 9. BSE convergence of the lowest direct exciton energy of undoped monolayer MoS_2 as well as the exciton binding energy as a function of the k-points grid.

According to the convergence of the *GW* quasiparticle band gap with respect to the energy cutoff of the dielectric matrix shown in Fig. 7(b), it is clear that an acceptable convergence is achieved at 10 Ry. As seen in Fig. 8, the static inverse dielectric function is almost the same for E_s=10 and 15 Ry. The calculated exciton binding energy changed by less than 10 meV when increasing the dielectric cutoff from 10 to 15 Ry. BSE calculations in Fig. 9 show a 48×48 × 1 k-points grid, mentioned in the main text, is well converged.

Finally, it is worth mentioning here that we used the same converged values of dielectric cutoff and k-point grid for monolayer WS_2 as similar convergence trends have already been reported for monolayer MoS_2 and WS_2 [22,37].

APPENDIX B: LONG WAVELENGTH LIMIT OF SCREENING

In order to calculate the static screening in the $q \to 0$ limit, we used the screened Coulomb potential identified by Czachor [38], $\frac{\exp(-K_{\mathrm{TF}} r)}{\epsilon_{\mathrm{p}} r}$, where both semiconductorlike (attributed to $\epsilon_{\mathrm{p}} = 1 + cte/E_{\mathrm{g}}^2$, where E_{g} denotes the energy gap) and metal-like (by introducing the Thomas-Fermi screening factor K_{TF}) contributions are included. Taking the 2D Fourier transformation [39], we obtain

$$V(\mathbf{q}) = \frac{2\pi}{2\epsilon_{\mathrm{p}}\Omega_{\mathrm{UC}}} \times \frac{1}{\sqrt{q^2 + K_{\mathrm{TF}}^2}}, \tag{B1}$$

where Ω_{UC} is the unit cell area, to fit to our numerical $W_{00}(\mathbf{q} \neq 0)$ data points. As seen in Fig. 10, the calculated data fit fairly well to Eq. (B1). We thus estimate $W_{00}(\mathbf{q} = 0) = 0.72$ and 0.56 bohr^{-1} for MoS_2 and WS_2, respectively.

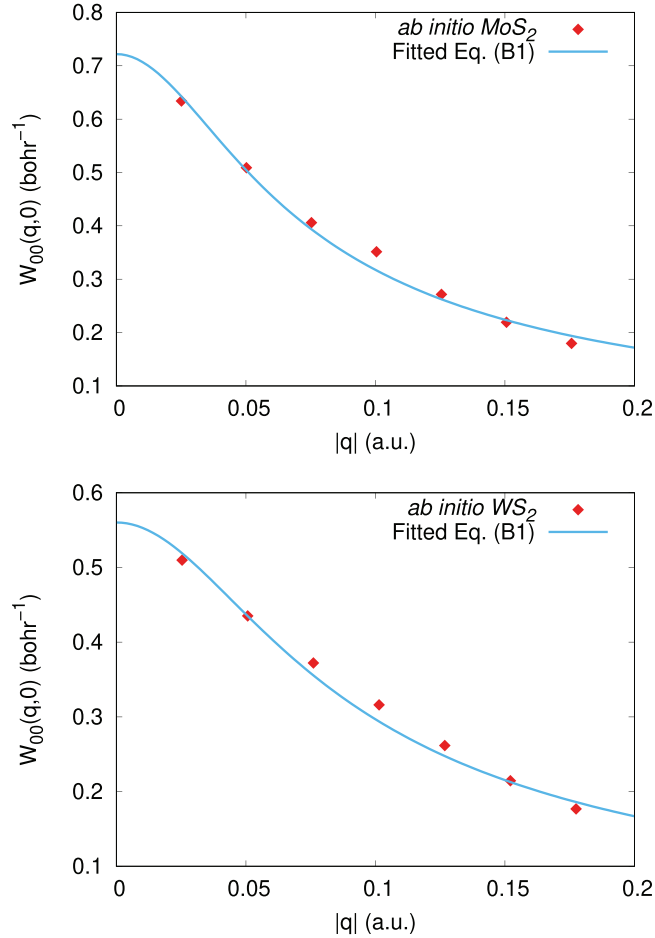

FIG. 10. Screened Coulomb potential for doped monolayer MoS_2 and WS_2 with $n_{\mathrm{e}} = 1.1 \times 10^{13}$ cm^{-2}. The dots represent the calculated W_{00} for several finite $|\mathbf{q}|$ while the continuous curve corresponds to Eq. (B1) fitted to the calculated data points.

[1] H. Wang, H. Yuan, S. Sae Hong, Y. Li, and Y. Cui, Physical and chemical tuning of two-dimensional transition metal dichalcogenides, Chem. Soc. Rev. **44**, 2664 (2015).

[2] X. Zhang, X. F. Qiao, W. Shi, J. B. Wu, D. S. Jiang, and P. H. Tan, Phonon and raman scattering of two-dimensional transition metal dichalcogenides from monolayer, multilayer to bulk material, Chem. Soc. Rev. **44**, 2757 (2015).

[3] A. Molina-Sánchez, K. Hummer, and L. Wirtz, Vibrational and optical properties of MoS_2: From monolayer to bulk, Surf. Sci. Rep. **70**, 554 (2015).

[4] D. Y. Qiu, F. H. da Jornada, and S. G. Louie, Screening and many-body effects in two-dimensional crystals: Monolayer MoS_2, Phys. Rev. B **93**, 235435 (2016).

[5] C. Tan, X. Cao, X. Wu, Q. He, J. Yang, X. Zhang, J. Chen, W. Zhao, S. Han, G. Nam, M. Sindoro, and H. Zhang, Recent advances in ultrathin two-dimensional nanomaterials, Chem. Rev. **117**, 6225 (2017).

[6] M. M Ugeda, A. J Bradley, S.-F. Shi, H. Felipe, Y. Zhang, D. Y Qiu, W. Ruan, S.-K. Mo, Z. Hussain, Z.-X. Shen, F. Wang, S. G. Louie, and M. F. Crommie, Giant bandgap renormalization and

excitonic effects in a monolayer transition metal dichalcogenide semiconductor, Nat. Mater. **13**, 1091 (2014).

[7] Z. Qiu, M. Trushin, H. Fang, I. Verzhbitskiy, S. Gao, E. Laksono, M. Yang, P. Lyu, J. Li, J. Su, M. Telychko, K. Watanabe, T. Taniguchi, J. Wu, A. H. C. Neto, L. Yang, G. Eda, S. Adam, and J. Lu, Giant gate-tunable bandgap renormalization and excitonic effects in a 2D semiconductor, Sci. Adv. **5**, eaaw2347 (2019).

[8] T. Kümmell, W. Quitsch, S. Matthis, T. Litwin, and G. Bacher, Gate control of carrier distribution in k-space in MoS_2 monolayer and bilayer crystals, Phys. Rev. B **91**, 125305 (2015).

[9] B. Chakraborty, J. Gu, Z. Sun, M. Khatoniar, R. Bushati, A. L. Boehmke, R. Koots, and V. M. Menon, Control of strong lightmatter interaction in monolayer WS_2 through electric field gating, Nano Lett. **18**, 6455 (2018).

[10] Y. Yu, Y. Yu, L. Huang, H. Peng, L. Xiong, and L. Cao, Giant gating tunability of optical refractive index in transition metal dichalcogenide monolayers, Nano Lett. **17**, 3613 (2017).

[11] K. F. Mak, K. He, C. Lee, G. H. Lee, J. Hone, T. F. Heinz, and J. Shan, Tightly bound trions in monolayer MoS_2, Nat. Mater. **12**, 207 (2013).

[12] Y. V. Zhumagulov, A. Vagov, N. Yu. Senkevich, D. R. Gulevich, and V. Perebeinos, Three-particle states and brightening of intervalley excitons in a doped MoS_2 monolayer, Phys. Rev. B **101**, 245433 (2020).

[13] S. Nojima, Dimensionality of exciton-state renormalization in highly excited semiconductors, Phys. Rev. B **51**, 11124 (1995).

[14] D. Van Tuan, B. Scharf, Z. Wang, J. Shan, K. F. Mak, I. Žutić, and H. Dery, Probing many-body interactions in monolayer transition-metal dichalcogenides, Phys. Rev. B **99**, 085301 (2019).

[15] F. Liu, M. E. Ziffer, K. R. Hansen, J. Wang, and X. Zhu, Direct Determination of Band-Gap Renormalization in the Photoexcited Monolayer MoS_2, Phys. Rev. Lett. **122**, 246803 (2019).

[16] F. Hüser, T. Olsen, and K. S. Thygesen, How dielectric screening in two-dimensional crystals affects the convergence of excited-state calculations: Monolayer MoS_2, Phys. Rev. B **88**, 245309 (2013).

[17] Y. Liang and L. Yang, Carrier Plasmon Induced Nonlinear Band Gap Renormalization in Two-Dimensional Semiconductors, Phys. Rev. Lett. **114**, 063001 (2015).

[18] S. Gao and L. Yang, Renormalization of the quasiparticle band gap in doped two-dimensional materials from many-body calculations, Phys. Rev. B **96**, 155410 (2017).

[19] S. Gao, Y. Liang, C. D. Spataru, and L. Yang, Dynamical excitonic effects in doped two-dimensional semiconductors, Nano Lett. **16**, 5568 (2016).

[20] R. W. Godby and R. J. Needs, Metal-Insulator Transition in Kohn-Sham Theory and Quasiparticle Theory, Phys. Rev. Lett. **62**, 1169 (1989).

[21] W. S. Yun, S. W. Han, S. C. Hong, In G. Kim, and J. D. Lee, Thickness and strain effects on electronic structures of transition metal dichalcogenides: 2H-MX_2 semiconductors (M = Mo, W; X = S, Se, Te), Phys. Rev. B **85**, 033305 (2012).

[22] H. Shi, H. Pan, Y.-W. Zhang, and B. I. Yakobson, Quasiparticle band structures and optical properties of strained monolayer MoS_2 and WS_2, Phys. Rev. B **87**, 155304 (2013).

[23] S. S. Ataei, D. Varsano, E. Molinari, and M. Rontani, Evidence of ideal excitonic insulator in bulk MoS_2 under pressure, Proc. Natl. Acad. Sci. USA **118**, e2010110118 (2021).

[24] J. P. Perdew, K. Burke, and M. Ernzerhof, Generalized Gradient Approximation made Simple, Phys. Rev. Lett. **77**, 3865 (1996).

[25] P. Giannozzi, S. Baroni, N. Bonini, M. Calandra, R. Car, C. Cavazzoni, D. Ceresoli, G. L. Chiarotti, M. Cococcioni, I. Dabo, A. D. Corso, S. de Gironcoli, S. Fabris, G. Fratesi, R. Gebauer, U. Gerstmann, C. Gougoussis, A. Kokalj, M. Lazzeri, L. Martin-Samos *et al.*, QUANTUM ESPRESSO: A modular and open-source software project for quantum simulations of materials, J. Phys.: Condens. Matter **21**, 395502 (2009); P. Giannozzi, O. Andreussi, T. Brumme, O. Bunau, M. B. Nardelli, M. Calandra, R. Car, C. Cavazzoni, D. Ceresoli, M. Cococcioni, N. Colonna, I. Carnimeo, A. D. Corso, S. de Gironcoli, P. Delugas, R. A. DiStasio, A. Ferretti, A. Floris, G. Fratesi, G. Fugallo *et al.*, Advanced capabilities for materials modelling with Quantum ESPRESSO, *ibid.* **29**, 465901 (2017); P. Giannozzi, O. Baseggio, P. Bonfà, D. Brunato, R. Car, I. Carnimeo, C. Cavazzoni, S. de Gironcoli, P. Delugas, F. Ferrari Ruffino, A. Ferretti, N. Marzari, I. Timrov, A. Urru, and S. Baroni, Quantum ESPRESSO toward the exascale, J. Chem. Phys. **152**, 154105 (2020).

[26] D. R. Hamann, Optimized norm-conserving Vanderbilt pseudopotentials, Phys. Rev. B **88**, 085117 (2013).

[27] X. Fan, D. J. Singh, and W. Zheng, Valence band splitting on multilayer MoS_2: Mixing of spinorbit coupling and interlayer coupling, J. Phys. Chem. Lett. **7**, 2175 (2016).

[28] Y. Zhang, H. Li, H. Wang, R. Liu, S.-L. Zhang, and Z.-J. Qiu, On valence-band splitting in layered MoS_2, ACS Nano **9**, 8514 (2015).

[29] G. Onida, L. Reining, and A. Rubio, Electronic excitations: Density-functional versus many-body Green's-function approaches, Rev. Mod. Phys. **74**, 601 (2002).

[30] M. S. Hybertsen and S. G. Louie, First-Principles Theory of Quasiparticles: Calculation of Band Gaps in Semiconductors and Insulators, Phys. Rev. Lett. **55**, 1418 (1985).

[31] A. Marini, C. Hogan, M. Grüning, and D. Varsano, yambo: An *ab initio* tool for excited state calculations, Comput. Phys. Commun. **180**, 1392 (2009); D. Sangalli, A. Ferretti, H. Miranda, C. Attaccalite, I. Marri, E. Cannuccia, P. Melo, M. Marsili, F. Paleari, A. Marrazzo, G. Prandini, P. Bonfà, M. O. Atambo, F. Affinito, M. Palummo, A. Molina-Sánchez, C. Hogan, M. Grüning, D. Varsano, and A. Marini, Many-body perturbation theory calculations using the YAMBO code, J. Phys.: Condens. Matter **31**, 325902 (2019).

[32] C. A. Rozzi, D. Varsano, A. Marini, E. K. U. Gross, and A. Rubio, Exact coulomb cutoff technique for supercell calculations, Phys. Rev. B **73**, 205119 (2006).

[33] Y. Li, A. Chernikov, X. Zhang, A. Rigosi, H. M. Hill, A. M. van der Zande, D. A. Chenet, E.-M. Shih, J. Hone, and T. F. Heinz, Measurement of the optical dielectric function of monolayer transition-metal dichalcogenides: MoS_2, $MoSe_2$, WS_2, and WSe_2, Phys. Rev. B **90**, 205422 (2014).

[34] A. Chernikov, A. M. van der Zande, H. M. Hill, A. F. Rigosi, A. Velauthapillai, J. Hone, and T. F. Heinz, Electrical Tuning of Exciton Binding Energies in Monolayer WS_2, Phys. Rev. Lett. **115**, 126802 (2015).

[35] K. Yao, A. Yan, S. Kahn, A. Suslu, Y. Liang, E. S. Barnard, S. Tongay, A. Zettl, N. J. Borys, and P. J. Schuck, Optically Discriminating Carrier-Induced Quasiparticle Band Gap and Exciton Energy Renormalization in Monolayer MoS_2, Phys. Rev. Lett. **119**, 087401 (2017).

[36] F. Bruneval and X. Gonze, Accurate GW self-energies in a plane-wave basis using only a few empty states: Towards large systems, Phys. Rev. B **78**, 085125 (2008).

[37] R. Frisenda, M. Drüppel, R. Schmidt, S. Michaelis de Vasconcellos, D. Perez de Lara, R. Bratschitsch, M. Rohlfing, and A. Castellanos-Gomez, Biaxial strain tuning of the optical properties of single-layer transition metal dichalcogenides, npj 2D Materials and Applications **1**, 10 (2017).

[38] A. Czachor, Dielectric function for a model, two-band semimetal, Phys. Rev. B **9**, 3357 (1974).

[39] G. Giuliani and G. Vignale, *Quantum Theory of the Electron Liquid* (Cambridge University, Cambridge, England, 2005).